Pharmaceutical Research, Vol. 23, No. 3, March 2006 (© 2006)
DOI: 10.1007/s11095-005-9571-z

Research Paper

A Mechanism-Based Integrated Pharmacokinetic Enzyme Model Describing the Time Course and Magnitude of Phenobarbital-Mediated Enzyme Induction in the Rat

Mats O. Magnusson,[1,2] Mats O. Karlsson,[1] and Rikard Sandström[1]

Received September 4, 2005; accepted November 21, 2005

Purpose. To characterize the magnitude, time course, and specificity of phenobarbital (PB)-mediated enzyme induction, and further, to develop an integrated pharmacokinetic (PK)-enzyme model describing the changes in the activities of CYP enzymes as well as in the PK of PB.
Methods. PB plasma concentrations and *in vitro* activities of several CYP enzymes were measured in rats treated with PB between 0 and 14 days. A PB PK-enzyme induction model was developed using the program NONMEM.
Results. PB treatment both induces and reduces the activity of CYP enzymes by stimulating the enzymes' formation or elimination rates. Certain CYP enzymes affected the PB PK through autoinduction. The half-life of the induction process was estimated to be 2 days for CYP1A2, CYP3A1/2, and CYP2B1/2, and 3 days for androstenedione producing enzymes. The CYP2C11 activity was rapidly reduced by PB treatment. A lag time for the PB autoinduction was observed. This lag time is explained by the rate difference between induction and reduction in CYP activities.
Conclusion. To our knowledge, this is the first example of an induction model that simultaneously describes plasma PK and *in vitro* data. It does so by integrating the bidirectional interaction between drug and enzymes in a mechanistic manner.

KEY WORDS: induction; modeling; NONMEM; phenobarbital; time course.

INTRODUCTION

The time course of enzyme induction is determined by the turnover rate of the induced enzyme. The enzyme concentration [E] can be calculated at any time during the induction process by the following equation (1):

$$[E] = [E_{induced}] - ([E_{induced}] - [E_{uninduced}]) \cdot e^{-k_{out} \cdot t}, \qquad (1)$$

where $[E_{induced}]$ is the concentration of the enzyme when fully induced, $[E_{uninduced}]$ is the baseline concentration of the enzyme, t is the time that elapsed since the start of the induction, and k_{out} is the first-order turnover rate constant of the enzyme. The turnover rate constant equals *ln* (2) divided by the half-life of the enzyme.

The time course of enzyme induction has been modeled in several studies (1–10). However, there are several aspects that should be considered in enzyme induction modeling, such as i) the part of the turnover model that should be affected by the inducing agent, ii) the shape of the inducing agent–induction magnitude relation, iii) how to handle the presence of a lag time, and iv) what data to use for measurement of enzyme induction. Following is a short review of these aspects.

i) The traditional view of the mechanism of enzyme induction is through *de novo* protein synthesis (1–3); therefore, most induction models act through stimulation of enzyme production (4–6). However, an increased enzyme concentration can also be the result of decrease in enzyme elimination through protein stabilization, which was the case in the ifosfamide model by Kerbusch *et al.* (7).

ii) The magnitude of the enzyme induction is most likely dependent on the concentration of the inducing compound, according to either a linear relation, as in the cyclophosphamide autoinduction model (5), or a nonlinear relation, as in the ifosfamide autoinduction model (7). There are also examples of step models where full induction occurs in the presence of the inducer and no induction in absence of it, as in the phenytoin autoinduction model (8).

iii) The presence of a lag time for the initiation of the induction has been observed in several studies. A suggested mechanism for the lag time is the chain of events required for protein synthesis. Therefore, a transduction model might be a

[1] Division of Pharmacokinetics and Drug Therapy, Department of Pharmaceutical Biosciences, Uppsala University, Box 591, SE-751 24, Uppsala, Sweden.
[2] To whom correspondence should be addressed. (e-mail: Mats.Magnusson@farmbio.uu.se)

ABBREVIATIONS: CYP, cytochrome P450; EROD, etoxyresorufin; i.p., intraperitoneal; k_{out}, turnover rate constant; OHT, hydroxytestosterone; PB, phenobarbital; PK, pharmacokinetics; R_{in}, production rate.

0724-8741/06/0300-0521/0 © 2006 Springer Science + Business Media, Inc.

suitable mechanistic way to model this, which was done in the artemisinin autoinduction model by Gordi *et al.* (9). However, more empirical models, such as a step function, where no induction occurs until a cutoff time point, have been used in the studies by Boddy *et al.* (4) and Frame and Beal (8).

iv) There can be several sources of data in the development of induction models. The most common data to use are plasma concentrations of a drug affected by the induction. Either the affected drug is the same as the drug causing the induction, i.e., autoinduction, or the inducer affects a separate drug, as in the phenobarbitone–nortriptyline model (6), where the changes in the elimination rate of nortriptyline over time were used as a measurement of enzyme induction. Sometimes metabolite data can be used to describe enzyme induction, as in the model presented by Hassan *et al.* (5), where metabolite data of the induced metabolic pathway were available. Alternative sources of data can be generated from an *in vitro* experiment, where the enzyme concentration is measured using real-time PCR or incubations with functional markers. An example of such an investigation was performed by Bomhard *et al.* (10), where the time course in the activities of several cytochrome P450 (CYP) enzymes were measured following dichlorobenzene treatment.

The aims of this study were to characterize the magnitude, time course, and specificity of phenobarbital (PB)-mediated enzyme induction and to develop an integrated pharmacokinetic-enzyme model describing the changes in the CYP enzymes' activities as well as the changes in the pharmacokinetics of PB over time. To accomplish this, we combined *in vitro* enzyme activity measurements with PB plasma concentrations from rats treated with the autoinducer PB for up to 14 days, thereby allowing a more mechanistic and explanatory model to be developed. Furthermore, consideration was made of the aspects (i)–(iii) described herein.

MATERIALS AND METHODS

Phenobarbital (Fenemal Recip® 200 mg/mL) for intravenous injections was purchased from the hospital pharmacy (Apoteket AB, Uppsala, Sweden). PB for standard preparations was purchased from Apoteket Production and Laboratory (Apoteket AB, Stockholm, Sweden). Methanol was purchased from JT Baker (Deventer, Holland) and was of gradient grade. Etoxyresorufin (EROD), resorufin, NADPH, sucrose, TRIS, EDTA, dithiothreitol and bovine serum albumin were purchased from Sigma Chemicals (St. Louis, MO, USA). Potassium pyrophosphate, glycerol, copper sulfate, sodium carbonate, sodium hydroxide pellets, and hydrochloric acid were supplied by Merck (Darmstadt, Germany). Water purification was done with a Milli-Q Academic system (Millipore, Bedford, MA, USA). 2α-, 6α-, 7α-, 16α-, 16β-Hydroxytestosterone (OHT), androstenedione, and testosterone were purchased from Steraloids Inc (Newport, RI, USA). 2β-OHT was purchased from Ultrafine Chemicals (Manchester, UK). All incubations with liver microsomes were performed in 0.1 M TRIS buffer (pH 7.4) containing 20% glycerol and 0.1 mM dithiothreitol.

Animal Treatment and Dosage of Inducer

Forty-four male Sprague–Dawley rats (Charles River, Uppsala, Sweden) weighing 250–300 g were used. The animals were acclimatized for at least 7 days prior to the experiment. They were maintained at 22°C in a humidity-controlled room with a 12-h light/dark cycle and free access to food and water. The animals were treated according to the "Principles of Laboratory Animal Care," and the Animal Ethics Committee at the court in Tierp, Sweden, approved the protocol (C195/1) before the study was initiated.

Forty of the rats were randomized into five groups of eight animals per group. The animals received intraperitoneal (i.p.) injections of PB (80 mg/kg body weight) once daily for 1, 2, 4, 9, and 14 consecutive days. Four rats were used as controls and received i.p. injections of saline. A 100-μL plasma sample was withdrawn from each animal daily. After the last dose of PB, ten plasma samples were withdrawn within the next 24 h. The rats were decapitated 24 h after their last injection of PB. The livers were harvested immediately after decapitation from four rats in each treatment group and from the four control animals. The livers were stored in TRIS buffer at −80°C until microsomes were extracted from the livers.

Preparation of Microsomes

Microsomes were extracted from 24 livers individually using different centrifugation steps according to the procedure described by Meijer *et al.* (11). The protein content in the microsome solution was determined in triplicates with the method developed by Lowry *et al.* (12) using bovine serum albumin as the standard. The microsomes were stored at −80°C until the measurements were to be conducted, whereupon they were incubated.

Microsome Incubations

The isolated microsomes were thawed on ice. Incubations were carried out at 37°C in a 60-rpm shaking water bath (Haake SWB 20, Fisons, Karlsruhe, Germany). The microsomes were added to a final protein concentration of 0.1 mg/mL in TRIS buffer containing 1 mg/mL NADPH. The incubation solution was preincubated for 3 min before the substrate was added. EROD and testosterone were added to final concentrations of 4 and 100 μM, respectively. The substrates were added in separate incubation vials. Incubations were also performed with the formed metabolites of EROD and testosterone with microsomes at the following concentrations (in μM): resorufin 0.1, 2α-OHT 1, 2β-OHT 0.4, 6α-OHT 0.85, 7α-OHT 0.5, 16α-OHT 0.26, 16β-OHT 0.4, and androstenedione 0.38. Incubations were conducted with the metabolites formed to enable calculation of the metabolic rate of these metabolites. These incubations were carried out in two separate incubation vials, with resorufin in one vial and all testosterone metabolites in another vial. Samples were taken from the incubation vials after 0, 10, 20, 30, and 40 min. The reactions were terminated by adding 100 μL of the sample to 200 μL methanol for the EROD and resorufin incubations and through a 1-min heat shock in water at 100°C for the

incubations with testosterone and its metabolites. After the reaction was terminated, the samples were centrifuged for 5 min at 7200 × *g* using a Force7 bench centrifuge (Denver Instrument Company) and the supernatant was transferred to Eppendorf tubes and stored at −20°C pending analysis.

Chemical Analysis

All of the analyses were conducted using high-pressure liquid chromatography (HPLC) systems consisting of a Triathlon refrigerated autosampler (Spark, Emmen, Holland) and LC-10AD pumps (Shimadzu, Kyoto, Japan). Quantification of PB plasma concentrations were done using a modified version of a previously reported method (13), here described briefly. An ultraviolet detector (Shimadzu SPD-10A) at wavelength 240 nm and a 10 × 4.6 mm, 5-μm particle size, Chromosphere C18 column (Thermo Hypersil, Runcorn, UK) was used to detect PB. The mobile phase consisted of 30% methanol in water. At a flow rate of 1.0 mL/min, PB was eluted after 11 min. PB was quantified using the peak area in standard curves obtained with blank rat plasma spiked to concentrations between 10 and 400 μM. All plasma samples were mixed with an equal volume of trichloroacetic acid; the mixture was centrifuged and 30 μL of the supernatant was injected into the HPLC system.

The resorufin was quantified using a method modified from Leclercq *et al.* (14), using a fluorescence detector (Jasco FP-920, Japan) and a 10 × 4.6 mm, 5-μm particle size C4 column (Thermo Hypersil). The mobile phase used in the resorufin analysis consisted of 58% 25 mM phosphate buffer (pH 7.0) and 42% methanol. The flow rate was 0.8 mL/min and the excitation and emission wavelengths were set at 530 and 580 nm, respectively. Resorufin was eluted from the column after 4.7 min and quantified using the area under the peaks in standard curves obtained for a series of concentrations of resorufin between 100 and 1500 nM. EROD has no emission at this wavelength and, therefore, was not quantified.

Testosterone and its metabolites were analyzed using an SPD-10A ultraviolet detector (Shimadzu) at wavelength 240 nm. However, a Quattro Ultima mass spectrometer (Micromass, Manchester, UK), was used as the detector for very low concentration samples. This analytical method is described in detail in a previous paper (15).

Data Analysis

The formation rates of the functional markers and the model that best describes the pharmacokinetics of PB and the induction processes were determined through nonlinear mixed-effect modeling using the first-order conditional estimation (FOCE) method with interaction in the computer program NONMEM, version VIβ (16). The estimated population model parameters were i) the fixed-effect parameters related to the typical individual and ii) the random-effect parameters, describing the magnitudes of interindividual variability in parameters (exponential models) and residual variability (proportional and/or additive models were employed) between individual predictions and observations. The difference in the objective function value produced by NONMEM was the main tool used to discriminate between two nested models. A drop in the objective function value of > 3.84 between two nested models corresponds to $p < 0.05$, which was regarded as statistically significant. In addition, the model-building process was guided by graphical evaluation using S-Plus v 6.1 (Insightful, Seattle, WA) with the Xpose library, version 3.1 (17), as well as a judgment of reasonable parameter estimates and their corresponding standard errors.

The model development was performed in two steps, described in detail in the next section. First the formation rates of the functional markers were estimated, and subsequently used as a measurement of enzyme activity in the integrated model. Then, an integrated model for simultaneous description of the time course in enzyme induction and the pharmacokinetics of PB was created.

Estimation of Formation Rates of Functional Markers

A linear metabolite concentration–time relation ($dM/dt = kS$) was not sufficient for estimating the formation rates of the different metabolites, as it would not take into account any sequential metabolism. Therefore, the formation rates were estimated as follows: First, the metabolic rates with which the metabolites resorufin, 2α-, 2β-, 6α-, 7α-, 16α-, and 16β-OHT, and androstenedione were metabolized were estimated as a first-order process Eq. (2). Then, on the basis of the incubations with EROD and testosterone, the formation rates of resorufin, 2α-, 2β-, 6α-, 7α-, 16α-, and 16β-OHT, and androstenedione were estimated using both the appearance of the metabolites Eq. (3) and the previously estimated metabolic rates (now fixed) of the metabolites Eq. (4). A decrease in formation rate, not attributable to a decrease in substrate levels, was observed during the 40-min incubation period, so a linear loss of enzyme activity over time was added to the model Eq. (5). The individual estimated initial formation rates of the functional markers (where Activity equals 1 at time 0) were used as measurements of enzyme activities in the further modeling process. Thereby, four data points (one per animal) were generated for each functional marker at induction days 0, 1, 2, 4, 9, and 14.

$$\frac{dM_1}{dt} = -k_{M0} M_1 \tag{2}$$

$$\frac{dS}{dt} = -k_{SM} S \times \text{Activity} \tag{3}$$

$$\frac{dM_2}{dt} = k_{SM} S \times \text{Activity} - k_{M0} M_2 \tag{4}$$

$$\frac{d(\text{Activity})}{dt} = -k \tag{5}$$

where M_1 is the concentration of metabolites during incubation with the metabolites, S is the concentration of substrate (EROD and testosterone), and M_2 is the concentration of metabolites during substrate incubations.

Modeling of Phenobarbital Pharmacokinetics

The population modeling was developed in steps. Initially, the pharmacokinetics of PB was modeled after a

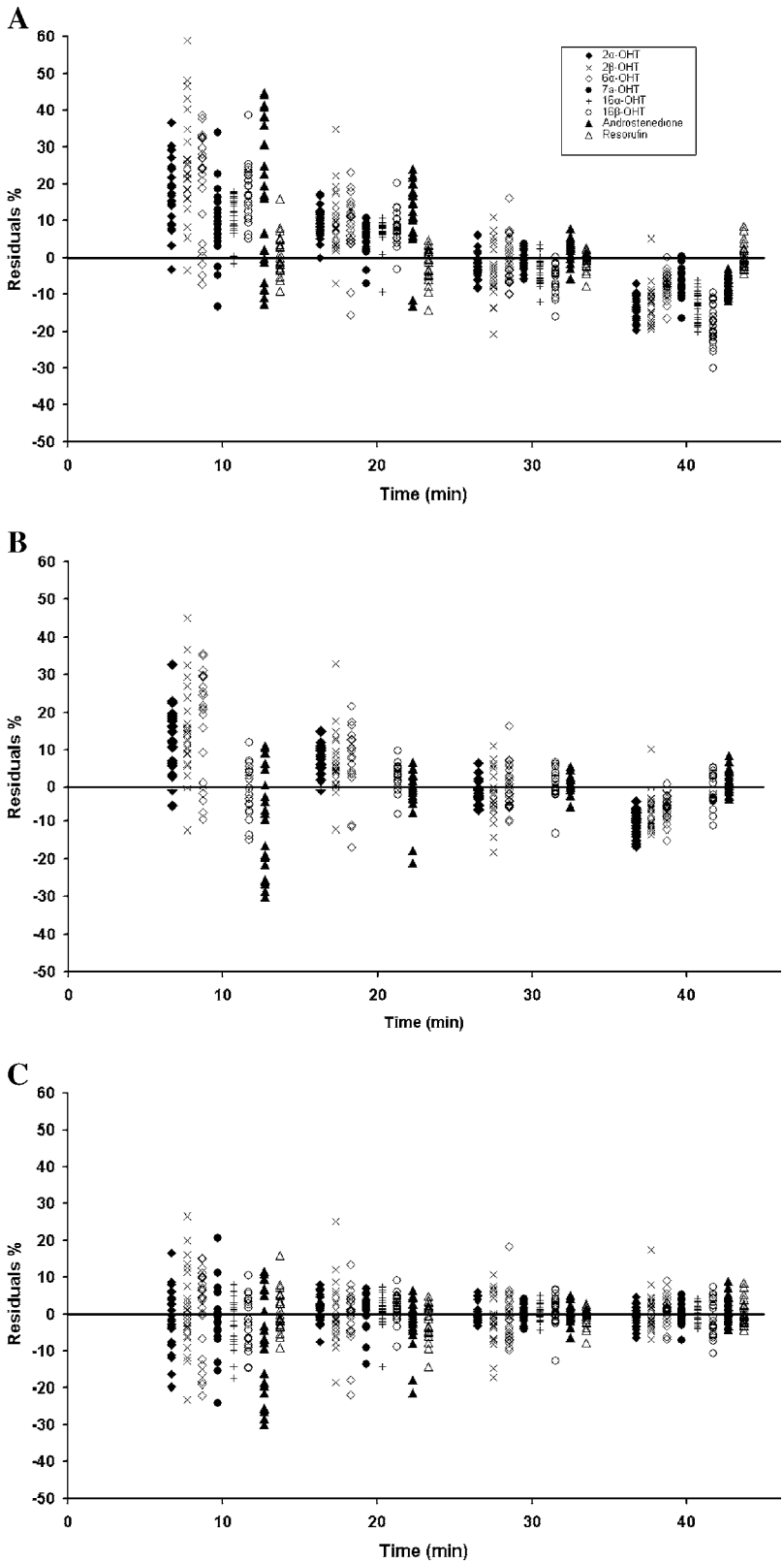

Fig. 1. Individual residuals (i.e., observed concentration − individual concentration predicted by the model) vs. incubation time: (A) using constant formation rate, (B) including sequential metabolism, and (C) including both linear loss of enzyme activity and sequential metabolism.

single PB dose, without an autoinduction model. One- and two-compartment structural models for the pharmacokinetics of PB were evaluated. Thereafter, data following repeated PB dosing was modeled, and an autoinduction model was introduced. Several autoinduction models were used, all consisting of two components: one for the pharmacokinetics of PB and one for the enzyme activity. The former component stimulated the production of enzymes, and the latter stimulated the elimination of PB. Three autoinduction models were evaluated, all dependent on the presence of PB: i) a step model, where one clearance value is used in the absence of PB and another value is used in the presence of PB [compare with Eq. (6)], ii) a linear model where PB clearance is linearly increased depending on the PB concentration in the central compartment [compare with Eq. (7)], and iii) a nonlinear model where PB clearance is nonlinearly dependent on the PB concentration in the central compartment [compare with Eq. (8)]. Both proportional [where $CL = CL_{Base}(1 + CL_{Induced})$] and additive forms (where $CL = CL_{Base} + CL_{Induced}$) were evaluated. Moreover, a lag time for the autoinduction to be initiated was observed. A step model (where the induction started at a time point later than the first dose of PB) as well as a transduction model (9,18), using two transition compartments causing a delay chain, were evaluated to describe the lag time.

When the model of the pharmacokinetics of PB and its autoinduction had been established, the influence of PB exposure on the activities of the different CYP enzymes was examined. The changes in the activities of the enzymes were modeled with turnover models. The effect of PB exposure on the production rate (R_{in}) and the turnover rates (k_{out}) of the enzymes was evaluated, comparing three PB-dependent models: a step model Eq. (6), a linear model Eq. (7), and nonlinear models Eqs. (8) and (9). In addition, the presence of a lag time for the induction was assessed:

$$R_{in} = R_{in,Base}\left(1 + \theta_{0/1} R_{in,induced}\right), \quad (6)$$

$$R_{in} = R_{in,Base}\left(1 + \theta C_p, \mathrm{PB}\right), \quad (7)$$

$$R_{in} = R_{in,Base}\left(1 + \frac{\mathrm{Ind}_{max} C_{p,PB}}{K_{m,Ind} + C_{p,PB}}\right), \quad (8)$$

$$k_{out} = k_{out,Base}\left(1 + \frac{\mathrm{Ind}_{max} C_{p,PB}}{K_{m,Ind} + C_{p,PB}}\right), \quad (9)$$

where R_{in} is the total formation rate, $R_{in,Base}$ is the uninduced formation rate, $k_{out,Base}$ is the uninduced turnover constant, $\theta_{0/1}$ is 0 in the absence of PB and 1 in the presence of PB, θ is a slope factor for the induction, Ind_{Max} is maximal induction, $C_{p,PB}$ is the concentration of PB in plasma, $K_{m,Ind}$ is the PB concentration causing 50% of maximal induction, and k_{out} is each enzyme's turnover constant.

As a final step, an integrated model, including the pharmacokinetics of PB, its effect on the activities of the CYP enzymes, and the influence of the CYP enzymes on the elimination of PB, was estimated simultaneously. Thereby, the autoinduction of PB was estimated via the PB-dependent changes in the activities of the enzymes. The CYP enzymes were included one by one to find which enzymes best described the autoinduction of PB elimination.

RESULTS

Estimation of Formation Rates and Metabolic Rates

Models using a constant value for the formation rate of the metabolites ($dM/dt = k \cdot S$) resulted in poor fits of the model predictions to the data as well as a negative trend in the individual residuals vs. incubation time plot (Fig. 1A). By introducing sequential metabolism of the metabolites a significantly improved fit was obtained (Fig. 1B). Moreover, a linear decline in enzyme activity during the 40-min incubation period was added to the model and resulted in symmetrically distributed individual residuals vs. incubation time plots (Fig. 1C). Logarithmic and exponential losses of enzyme activity during the incubation period were also evaluated, but these models did not improve the fit of the model to the observed data. The final model, using the data for further metabolism and a linear decline in enzyme activity, resulted in concentration–time curves that fitted well with the observed data (Fig. 3C and D).

All the formed metabolites were further metabolized (data not presented) apart from resorufin and 7α-OHT for which metabolism could not be detected. Further metabolism of 2α-, 16α-OHT and androstenedione increased due to PB exposure, resulting in a 2- to 3-fold induction in the metabolic rate from day 0 to day 14. 2β-, 6α-, 16β-OHT had comparable metabolic rates throughout the study period. The estimation of the metabolic rate of 16α-OHT was uncertain, probably due to fast metabolism of this compound.

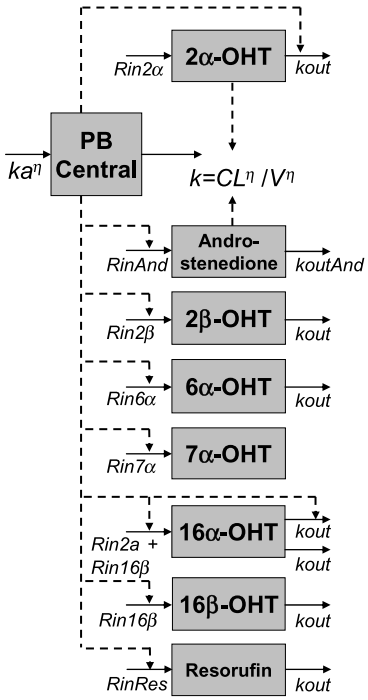

Fig. 2. Schematic diagram of the final model. Solid arrows indicate flows. Dashed arrows indicate where the amount of one compartment increases the inflow or outflow from another compartment, or clearance of PB. η indicates where interindividual variability was applied in the model.

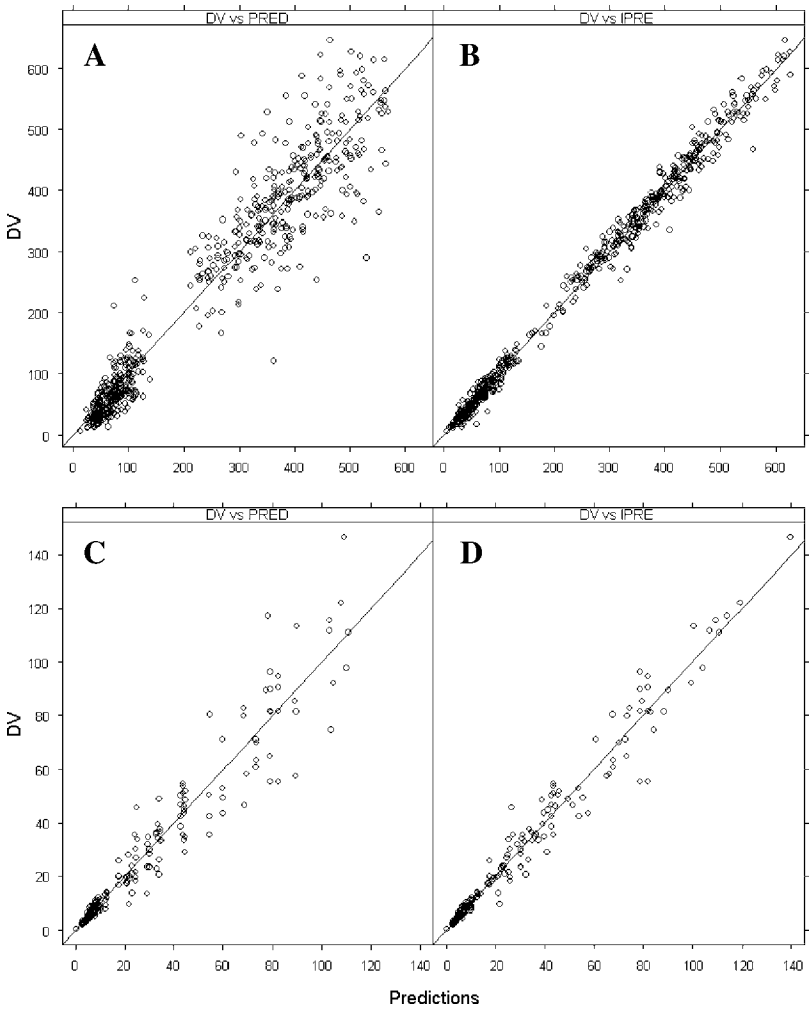

Fig. 3. (A) Observed PB concentrations (DV) and (C) functional marker formation rates (DV) vs. model predicted (PRED) and (B) observed PB concentrations (DV) and (D) functional marker formation rates (DV) vs. individual model predictions (IPRED).

Enzyme Kinetics

The final model consisted of one central PB compartment and eight enzyme-activity compartments (Fig. 2). The model described the observed data well (Figs. 3 and 4). The amount of PB in the central compartment influenced the enzyme activity through a nonlinear relation Eqs. (8) and (9) for all enzymes except 7α-OHT, where a step function was used instead Eq. (6). The same $K_{m,Ind}$ value of the induction process was used for all enzymes and was estimated to be 13.5 μmol. The maximal change in formation rate of each functional marker is presented in Table I.

PB treatment was found to induce the formation rates of several functional markers, but it also reduced the formation rates of 2α- and 16α-OHT (Fig. 4). The induction of the formation rates of resorufin and 2β-, 6α-, and 16β-OHT followed a monoexponential time course with no significant lag time for the induction to start, Fig. 4. PB exposure increased the production rate (Rin) of all of these induced enzymes according to Eq. (8). The turnover rate kout was estimated to be 0.355 days^{-1}, corresponding to a half-life of 2 days, for these functional markers. The induction of the formation rates of androstenedione also followed a monoexponential trend, but with a kout of 0.235 days^{-1}, corresponding to a half-life of 3 days. The induction of the 7α-OHT-forming enzyme was linearly increased over time.

The 2α-OHT formation rate was reduced following PB treatment. This decrease in activity was modeled as an increase turnover rate (k_{out}) of the 2α-OHT-producing enzyme Eq. (9). 16α-OHT is formed by the enzymes forming 16β-OHT and 2α-OHT; thus, the changes in the 16α-OHT formation rate were modeled as a combination of the formation rates of 16β- and 2α-OHT.

PB Pharmacokinetics and Autoinduction

A one-compartment model was sufficient to describe the PK of PB. The PK parameters of PB are presented in Table I. The PB clearance and volume of distribution was estimated to be 17.4 L/h and 0.24 L, respectively, resulting

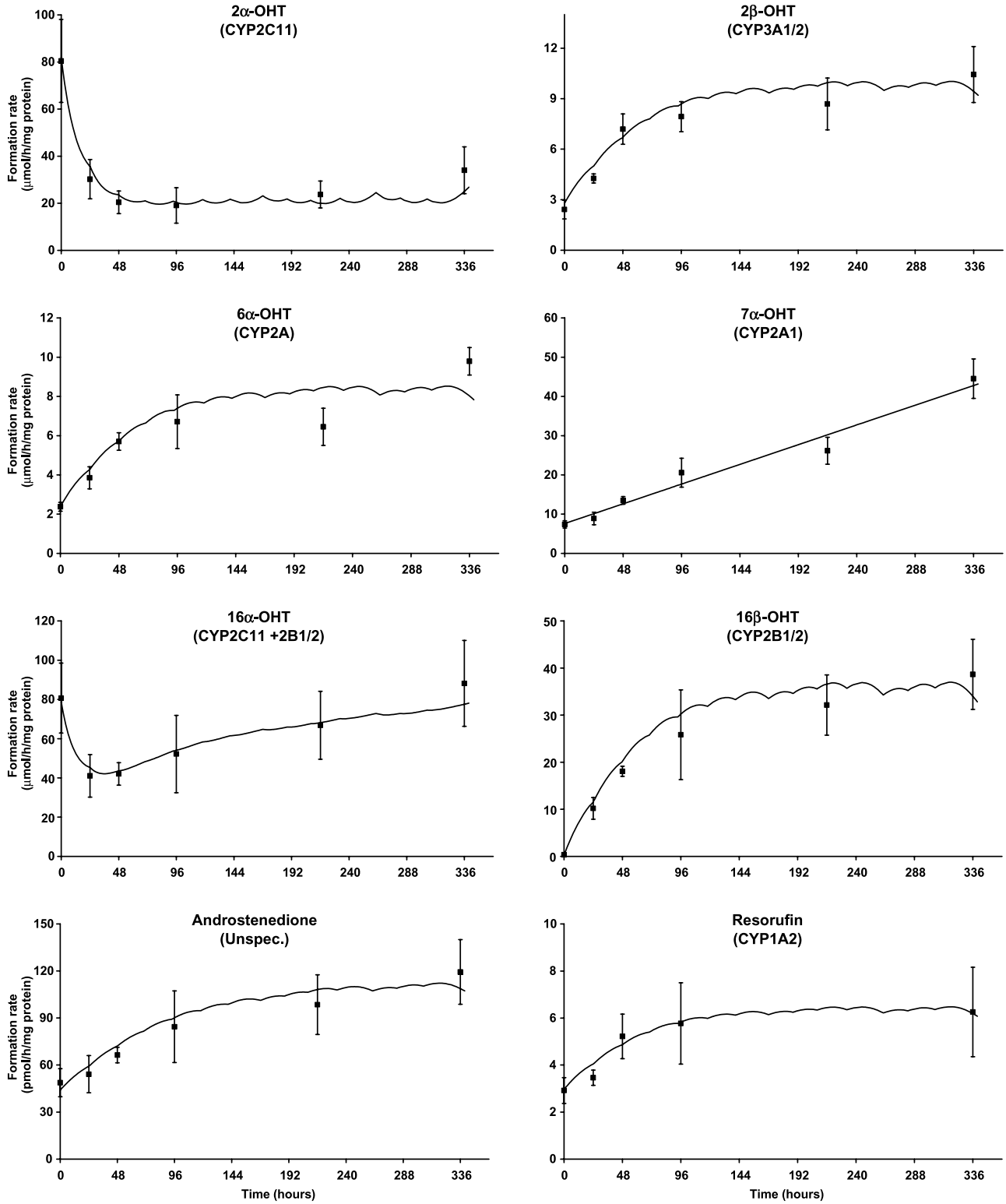

Fig. 4. Model-predicted time course and magnitude of the formation rate of the functional markers, and observed average ± SD enzyme activity of each functional marker at each time point.

in a half-life for the compound of about 10 h in the uninduced state. The time course and magnitude of the autoinduction of PB were best described using the combined changes in the activities of the 2α-OHT- and androstenedione-producing enzymes (see the Appendix for the differential equations). Figure 6 shows the estimated changes in PB clearance over time in a typical individual. The model could well describe the observed PB data (Figs. 3A, B, and 5).

Table I. Typical Values [Relative Standard Errors (RSE %)] of Pharmacokinetic (PK) Parameters for Phenobarbital (PB), the Induction in the Formation Rates of the Functional Markers, and the Interindividual Variability (IIV) (RSE %) of the Parameters

Parameter	Estimate (RSE %)	IIV % (RSE %)
PK parameters		
Volume (L)	0.240 (1.7)	11 (43)
Clearance (mL/h)	17.4 (3.8)	17 (23)
k_a (h^{-1})	5.54 (22)	90 (33)
$K_{m,Ind}$ (μmol)	13.5 (68)	
k_{out} (24 h^{-1})	0.355 (14)	
k_{out} androstenedione (24 h^{-1})	0.235 (14)	
Ind_{max} 2α-OHT[a]	4.05 (24)	
Ind_{max} 2β-OHT[b]	3.60 (25)	28 (41)[c]
Ind_{max} 6α-OHT[b]	3.54 (25)	[c]
Induction slope 7α-OHT	0.105 (6.4)	
Ind_{max} 16β-OHT[b]	152 (21)	[c]
Ind_{max} androstenedione[b]	2.26 (26)	[c]
Ind_{max} resorufin[b]	1.63 (35)	[c]
Residual error		
PB (%)	5.20 (12)	0.12
PB (μM)	10.1 (9.7)	0.097
2α-OHT[d] (SD)	9.16 (19)	0.19
2β-OHT[d] (SD)	0.852 (12)	0.12
6α-OHT[d] (SD)	0.764 (18)	0.18
7α-OHT[d] (SD)	3.46 (17)	0.17
16β-OHT (%)	6.72 (37)	0.37
Androstenedione[d] (SD)	7.90 (11)	0.11
Resorufin[e] (SD)	1.04 (19)	0.19

[a] Ind_{max} value in Eq. (9). A value of 0 indicates no induction.
[b] Ind_{max} value in Eq. (8). A value of 0 indicates no induction.
[c] The same IIV of 28% was used for all Ind_{max} values.
[d] Values are in micromoles per hour per milligram protein.
[e] Values are in picomoles per hour per milligram protein.

DISCUSSION

Formation Rate of Functional Markers

The functional markers used here are considered to be associated with the following CYP enzymes: CYP1A2 for resorufin (19), CYP3A1/2 for 2β-OHT (20,21), partly CYP2A for 6α-OHT (22,23), and CYP2B1/2 for 16β-OHT (20,24). According to the turnover concept, the time it takes to reach half of the maximal enzyme induction is equivalent to each of the enzymes' half-lives, which here was estimated to be 47 h for the CYP1A2, CYP3A, and CYP2B enzymes. This half-life is in good agreement with previously reported half-lives for these CYP enzymes (25).

Androstenedione is a quite unspecific functional marker proposed to be associated with CYP2B1/2 and CYP2C11 activity (23,26). The induction in the formation rate of androstenedione was significantly slower than for the other compounds, with an estimated half-life of 72 h. One explanation for the long apparent half-life could be that more than one enzyme is involved in this metabolism. However, the involvement of multiple enzymes with different half-lives would result in a multiple exponential curve for the androstenedione induction, which was not observed in this study.

The change in the formation rate of 7α-OHT is thought to be caused by changes in the activity of CYP2A1 (22,27,28). The formation rate of 6α-OHT is also considered to at least partly be a measurement of this enzyme's activity. However, the formation rate of 6α-OHT follows the same monoexponential induction as thed other functional markers, whereas that of 7α-OHT does not. We do not fully understand the reason for this difference, but it could be the result of poor substrate specificity. The linear increase in the formation rate of 7α-OHT could be caused by the long half-life for this enzyme, where only the onset of the monoexponential curve has been studied here.

The decrease in the formation rates of 2α- and 16α-OHT was very rapid. The decrease in the formation rate of 2α-OHT is thought to be caused by a decrease in the activity of CYP2C11, whereas 16α-OHT is formed both by CYP2C11 and by CYP2B1/2 (20,23). There was no PB present in the incubation vials, and competitive binding can therefore not explain the decrease in CYP2C11 activity. It has been proposed that the decrease in CYP2C11 expression might be caused by reduced production of the enzyme due to decrease in the amplitude of growth hormone pulses caused by PB treatment (29), but the exact mechanism is not known. If PB only affects the production of this enzyme, the half-life of CYP2C11 must be less than 12 h to fit the rapid decline in the enzyme activity. We find it unlikely that the half-life of this enzyme is four times shorter than any other enzyme here investigated. The inhibition of CYP2C11 was therefore modeled as an increased elimination of the enzyme (k_{out}). An increased kout results in both a decrease in enzyme concentration and a more rapid change in the enzyme activity and fitted well with the observed data.

The amount of PB in the central compartment affected the enzyme activity through a nonlinear relation Eqs. (8) and (9) for all enzymes except 7α-OHT. The same $K_{m,Ind}$ value was used for all induction processes, which is a reasonable modeling assumption, as enzyme induction is the result of PB binding the same nuclear receptor. It is therefore logical that they have the same $K_{m,Ind}$ value, which would correspond to the affinity of PB to the nuclear receptor. The $K_{m,Ind}$ value in this single-dose-level study was quite uncertain with a relative standard error of 68%. The certainty of the $K_{m,Ind}$ value for the induction could probably be increased with an increased number of dose levels.

Pharmacokinetics of Phenobarbital and the Autoinduction Process

The autoinduction in the pharmacokinetics of PB was initially modeled using an empirical model where the half-life of the autoinduction process was estimated to be 74 h, with a 42 h delay for the autoinduction of PB to be initiated. We assumed that the delayed onset of the autoinduction was the result of the many steps necessary in the synthesis of new proteins and, therefore, we expected to see similar lag times for the onset of the induction in the *in vitro* experiments. However, no significant lag time could be observed for the induction of any of the functional markers (Fig. 4). We then found that PB treatment both induced and reduced the activity of different CYP enzymes and that the time course of the enzyme induction was much slower than the reduction.

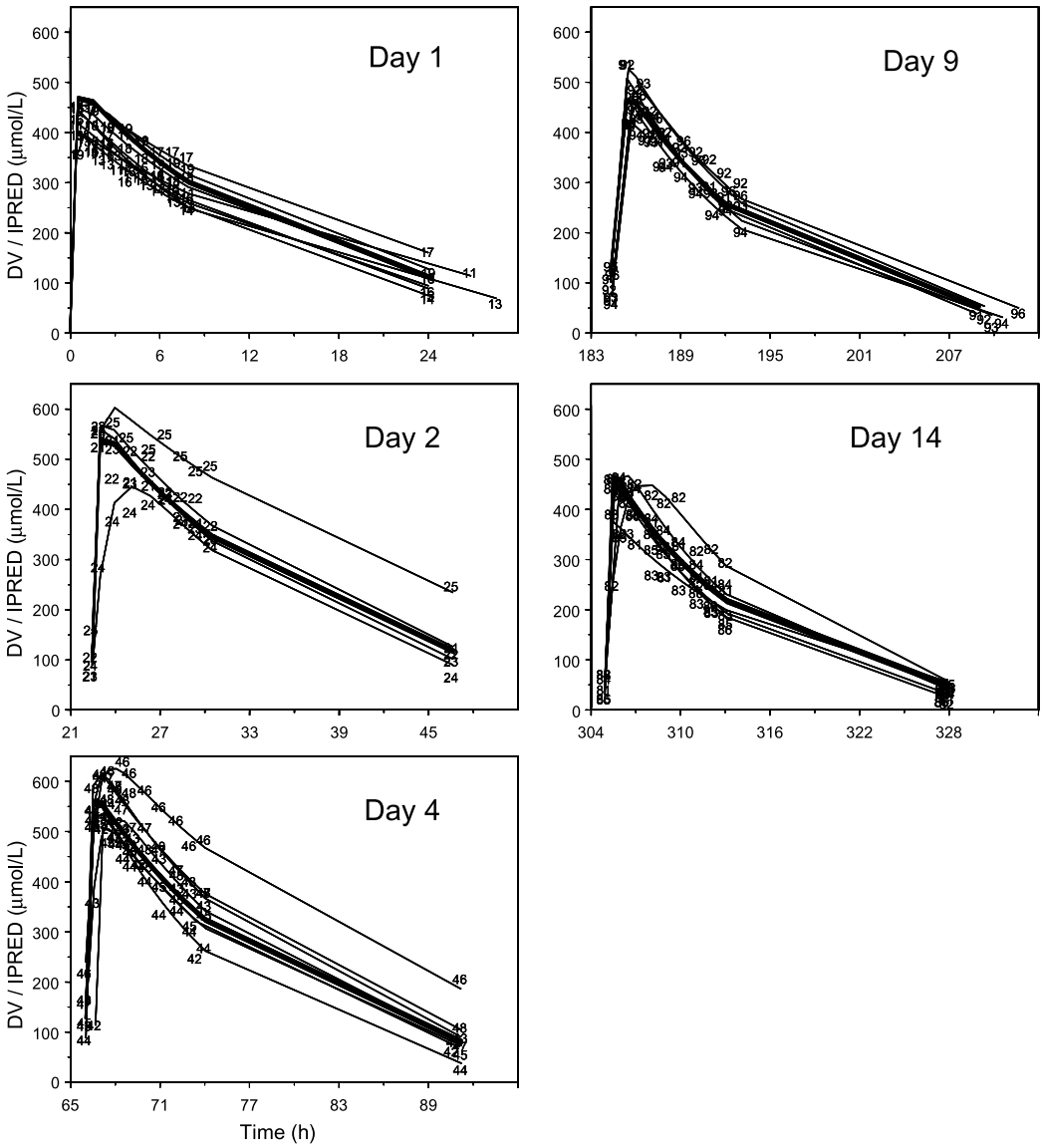

Fig. 5. Numbers represent observed PB concentrations (DV), the solid line represents individual model predicted concentrations (IPRED), and the thick solid line represents the model prediction for a typical individual (PRED) vs. time. Only the days with frequent data sampling are shown.

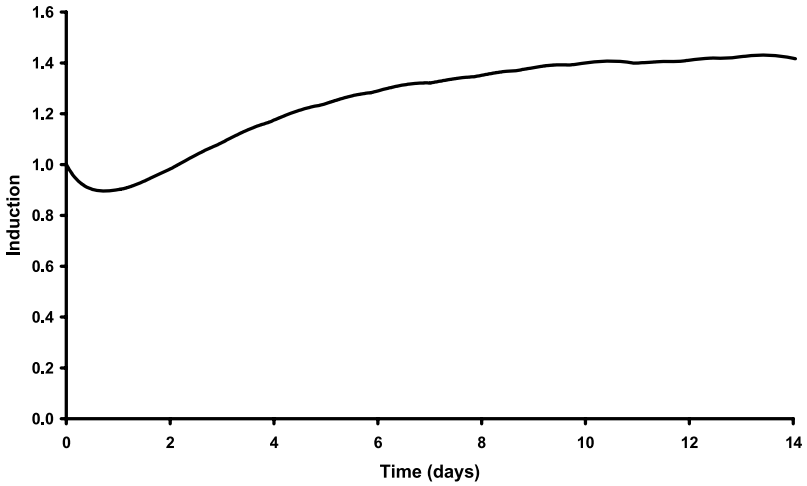

Fig. 6. The solid line shows fold induction vs. time for the typical individual (1 equals no induction).

The combined changes in the formation rate of 2α-OHT and androstenedione could well mimic both the time course of the autoinduction and its delayed onset. The apparent lag time for the onset of the PB autoinduction could be explained by the fast reduction in formation rate of 2α-OHT and the slower androstenedione induction. Figure 6 shows the time course of the autoinduction in a typical individual. Clearly, a fast inhibition of CYP2C11 in combination with a slower induction can cause the apparent lag time for the onset of the induction. As support for the mechanistic model, where *in vitro* incubations explained the PB autoinduction, the objective function values were comparable between the empirical and the mechanistic models, although the number of parameters was reduced in the mechanistic model. In addition, the mechanistic model was much more stable and faster to run than the empirical model.

The metabolic pattern of PB is not fully understood in humans and even less characterized in the rat. In humans, PB is metabolized by CYP2C9, CYP2C19, and CYP2E1; it undergoes N-glucosylation and is renally excreted (30–33). We do not claim that PB only is metabolized by the enzymes forming 2α-OHT and androstenedione. However, the changes in the formation rates of these functional markers could well describe the time course of the PB autoinduction process and could give a mechanistic explanation to the observed lag time for the onset of the PB autoinduction. We thereby show that *in vitro* generated data can contribute valuable information in the development of induction models. Together with a better understanding of which enzymes are involved in a drug's metabolism and with more specific enzyme-activity measurements, the methods used in this study could result in even better models.

Modeling of the Formation Rates of the Functional Markers

In this study, the formation rates of the functional markers were estimated, rather than calculated by the amount of metabolite formed during a certain period. The reason for this was that we wanted to take into account the metabolic rate of the metabolites formed. It is well known that PB not only induces phase I metabolism through CYP enzymes, but it can also induce phase II metabolism (34,35). It was, therefore, necessary to follow the PB-mediated changes in the further metabolism of the metabolites formed. The inclusion of data of further metabolism significantly improved the model, showing that these data contain important information. However, the sequential metabolism of the metabolites formed could not fully explain the bent concentration–time curve. By estimating a linear decrease in enzyme activity over time, well-fitted concentration–time curves could be obtained and the enzyme activity could be calculated. An explanation to the loss in activity could be that the formed metabolites reduce the enzyme activity at later time points. This explanation is supported by the fact that the decline in formation rate differed for the compounds used. By estimating the linear decline in enzyme activity, all data points collected during the 40-min incubations could be used. An alternative approach would have been to only use the concentrations of the metabolites formed during the first 10 to 20 min, where the formation of the metabolites was almost linear. However, this would probably have resulted in less reliable formation rate estimates for the functional markers.

In summary, we have in this study followed the pharmacokinetics of PB, its autoinduction process, and the time course of PB-mediated changes in several CYP enzyme activities by use of rat liver microsomes and functional markers. Both the rates with which CYP functional markers were formed and further metabolized were modeled using NONMEM. In addition, a mechanistic model describing the PB autoinduction process as well as the PB-dependent changes in the formation rate of the functional makers was developed in NONMEM. The final model describes the pharmacokinetics of PB in the rat during repeated i.p. PB dosing, as well as the time course of the changes of several CYP functional markers. Moreover, the changes in the formation rate of 2α-OHT and androstenedione explains the magnitude and the time course, including the lag time of the PB autoinduction. To our knowledge, this is the first example of a model that simultaneously describes plasma PK and formation rates of functional markers. It does so by integrating the bidirectional interaction between drug and enzymes in a mechanistic manner.

ACKNOWLEDGMENTS

We are grateful to Britt Jansson for assistance in the laboratory and to Kjell Wikvall and Siv Jönsson for valuable comments on the work.

REFERENCES

1. R. H. Levy, A. A. Lai, and M. S. Dumain. Time-dependent kinetics IV: pharmacokinetic theory of enzyme induction. *J. Pharm. Sci.* **68**:398–399 (1979).
2. A. B. Okey. Enzyme induction in the cytochrome P-450 system. *Pharmacol. Ther.* **45**:241–298 (1990).
3. J. Y. Chien, K. E. Thummel, and J. T. Slattery. Pharmacokinetic consequences of induction of CYP2E1 by ligand stabilization. *Drug Metab. Dispos.* **25**:1165–1175 (1997).
4. A. V. Boddy, M. Cole, A. D. Pearson, and J. R. Idle. The kinetics of the auto-induction of ifosfamide metabolism during continuous infusion. *Cancer Chemother. Pharmacol.* **36**:53–60 (1995).
5. M. Hassan, U. S. Svensson, P. Ljungman, B. Bjorkstrand, H. Olsson, M. Bielenstein, M. Abdel-Rehim, C. Nilsson, M. Johansson, and M. O. Karlsson. A mechanism-based pharmacokinetic-enzyme model for cyclophosphamide autoinduction in breast cancer patients. *Br. J. Clin. Pharmacol.* **48**:669–677 (1999).
6. C. von Bahr, E. Steiner, Y. Koike, and J. Gabrielsson. Time course of enzyme induction in humans: effect of pentobarbital on nortriptyline metabolism. *Clin. Pharmacol. Ther.* **64**:18–26 (1998).
7. T. Kerbusch, A. D. Huitema, J. Ouwerkerk, H. J. Keizer, R. A. Mathot, J. H. Schellens, and J. H. Beijnen. Evaluation of the autoinduction of ifosfamide metabolism by a population pharmacokinetic approach using NONMEM. *Br. J. Clin. Pharmacol.* **49**:555–561 (2000).
8. B. Frame and S. L. Beal. Non-steady state population kinetics of intravenous phenytoin. *Ther. Drug Monit.* **20**:408–416 (1998).
9. T. Gordi, R. Xie, N. V. Huong, D. X. Huong, M. O. Karlsson, and M. Ashton. A semiphysiological pharmacokinetic model for artemisinin in healthy subjects incorporating autoinduction of metabolism and saturable first-pass hepatic extraction. *Br. J. Clin. Pharmacol.* **59**:189–198 (2005).
10. E. M. Bomhard, U. Schmidt, and E. Loser. Time course of enzyme induction in liver and kidneys and absorption, distribu-

tion and elimination of 1,4-dichlorobenzene in rats. *Toxicology* **131**:73–91 (1998).
11. J. Meijer, A. Bergstrand, and J. W. DePierre. Preparation and characterization of subcellular fractions from the liver of C57B1/6 mice, with special emphasis on their suitability for use in studies of epoxide hydrolase activities. *Biochem. Pharmacol.* **36**:1139–1151 (1987).
12. O. Lowry, N. Rosebrough, L. Farr, and R. Randall. Protein measurement with the Folin phenol reagent. *J. Biol. Chem.* **193**:265–275 (1951).
13. K. Kushida, K. Chiba, and T. Ishizaki. Simultaneous liquid chromatographic determination of chloramphenicol and antiepileptic drugs (phenobarbital, phenytoin, carbamazepine, and primidone) in plasma. *Ther. Drug Monit.* **5**:127–133 (1983).
14. I. Leclercq, J. P. Desager, C. Vandenplas, and Y. Horsmans. Fast determination of low-level cytochrome P-450 1A1 activity by high-performance liquid chromatography with fluorescence or visible absorbance detection. *J. Chromatogr., B Biomed. Appl.* **681**:227–232 (1996).
15. M. O. Magnusson and R. Sandström. Quantitative analysis of eight testosterone metabolites using column switching and liquid chromatography/tandem mass spectrometry. *Rapid Commun. Mass Spectrom.* **18**:1089–1094 (2004).
16. S. L. Bealand and L. S. Sheiner. *NONMEM user's guide, NONMEM Project Group*, University of California at San Francisco, 1994.
17. E. N. Jonsson and M. O. Karlsson. Xpose-an S-PLUS based population pharmacokinetic/pharmacodynamic model building aid for NONMEM. *Comput. Methods Programs Biomed.* **58**:51–64 (1999).
18. Y. N. Sun, D. C. DuBois, R. R. Almon, and N. A. Pyszczynski, and W. J. Jusko. Dose-dependence and repeated-dose studies for receptor/gene-mediated pharmacodynamics of methylprednisolone on glucocorticoid receptor down-regulation and tyrosine aminotransferase induction in rat liver. *J. Pharmacokinet. Biopharm.* **26**:619–648 (1998).
19. A. D. Rodrigues and R. A. Prough. Induction of cytochromes P450IA1 and P450IA2 and measurement of catalytic activities. *Methods Enzymol.* **206**:423–431 (1991).
20. D. J. Waxman. Interactions of hepatic cytochromes P-450 with steroid hormones. Regioselectivity and stereospecificity of steroid metabolism and hormonal regulation of rat P-450 enzyme expression. *Biochem. Pharmacol.* **37**:71–84 (1988).
21. S. Imaoka, T. Yamada, T. Hiroi, K. Hayashi, T. Sakaki, Y. Yabusaki, and Y. Funae. Multiple forms of human P450 expressed in *Saccharomyces cerevisiae*. Systematic characterization and comparison with those of the rat. *Biochem. Pharmacol.* **51**:1041–1050 (1996).
22. A. J. Sonderfan, M. P. Arlotto, D. R. Dutton, S. K. McMillen, and A. Parkinson. Regulation of testosterone hydroxylation by rat liver microsomal cytochrome P-450. *Arch. Biochem. Biophys.* **255**:27–41 (1987).
23. D. E. Ryan and W. Levin. Purification and characterization of hepatic microsomal cytochrome P-450. *Pharmacol. Ther.* **45**:153–239 (1990).
24. D. J. Waxman, A. Ko, and C. Walsh. Regioselectivity and stereoselectivity of androgen hydroxylations catalyzed by cytochrome P-450 isozymes purified from phenobarbital-induced rat liver. *J. Biol. Chem.* **258**:11937–11947 (1983).
25. A. Parkinson, P. E. Thomas, D. E. Ryan, and W. Levin. The *in vivo* turnover of rat liver microsomal epoxide hydrolase and both the apoprotein and heme moieties of specific cytochrome P-450 isozymes. *Arch. Biochem. Biophys.* **225**:216–236 (1983).
26. A. W. Wood, D. C. Swinney, P. E. Thomas, D. E. Ryan, P. F. Hall, W. Levin, and W. A. Garland. Mechanism of androstenedione formation from testosterone and epitestosterone catalyzed by purified cytochrome P-450b. *J. Biol. Chem.* **263**:17322–17332 (1988).
27. K. Kobayashi, K. Urashima, N. Shimada, and K. Chiba. Substrate specificity for rat cytochrome P450 (CYP) isoforms: screening with cDNA-expressed systems of the rat. *Biochem. Pharmacol.* **63**:889–896 (2002).
28. W. Levin, P. E. Thomas, D. E. Ryan, and A. W. Wood. Isozyme specificity of testosterone 7 alpha-hydroxylation in rat hepatic microsomes: is cytochrome P-450a the sole catalyst?. *Arch. Biochem. Biophys.* **258**:630–635 (1987).
29. D. J. Waxman, N. A. Pampori, P. A. Ram, A. K. Agrawal, and B. H. hapiro. Interpulse interval in circulating growth hormone patterns regulates sexually dimorphic expression of hepatic cytochrome P450. *Proc. Natl. Acad. Sci. USA* **88**:6868–6872 (1991).
30. P. Reidenberg, P. Glue, C. R. Banfield, R. D. Colucci, J. W. Meehan, E. Radwanski, P. Mojavarian, C. C. Lin, J. Nezamis, M. Guillaume, and M. B. Affrime. Effects of felbamate on the pharmacokinetics of phenobarbital. *Clin. Pharmacol. Ther.* **58**:279–287 (1995).
31. R. Riva, F. Albani, M. Contin, and A. Baruzzi. Pharmacokinetic interaction between antiepileptic drugs. *Clin. Pharmacokinet.* **31**:470–493 (1995).
32. G. D. Anderson. A mechanistic approach to antiepileptic drug interactions. *Ann. Pharmacother.* **32**:554–563 (1998).
33. S. G. Paibir, W. H. Soine, D. F. Thomas, and R. A. Fisher. Phenobarbital N-glucosylation by human liver microsomes. *Eur. J. Drug Metab. Pharmacokinet.* **29** 1:51–59 (2004).
34. P. Bentley and F. Oesch. Foreign compound metabolism in the liver. *Prog. Liver Dis.* **7**:157–178 (1982).
35. I. S. Owens. Genetic regulation of UDP-glucuronosyltransferase induction by polycyclic aromatic compounds in mice. Cosegregation with aryl hydrocarbon (benzo(alpha)pyrene) hydroxylase induction. *J. Biol. Chem.* **252**:2827–2833 (1977).

```
$PK
;;;;;;PB KINETICS
V                  = THETA(1) *EXP(ETA(1))
TVCL               = THETA(2)*EXP(ETA(2))
TVKA               = THETA(3)*EXP(ETA(4))

;;;;;;INDUCTION RESORUFIN
T12RES =THETA(4)              ;Half life of the Resorufin producing enzyme
KRES =0.6931/T12RES
RINRES = THETA(9)             ;Uninduced formation rate of Resorufin producing enzyme
INDRES = THETA(10)*EXP(ETA(3));Inducability of Resorufin producing enzyme
A_0(3) = RINRES/KRES          ;A_0(3) is uninduced formation rate of Resorufin (observed
in in vitro experiment)

;;;;;;INHIBITION 2α-OHT
T122A =THETA(4)               ;Half life of the 2α OHT producing enzyme
K2A =0.6931/T122A
RIN2A = THETA(13)             ;Uninhibited formation rate of 2α OHT producing enzyme
IND2A = THETA(14)             ;Inhibition of 2α OHT producing enzyme
A_0(4) = RIN2A/K2A            ;A_0(4) is uninhibited formation rate of 2A OHT (observed
in in vitro experiment)

;;;;;;INDUCTION 2β, 6α, 16β-OHT and androstenedione was done as for resorufin induction

;;;;;; INDUCTION 7α-OHT
A_0(7) = THETA(15)            ;A_0(7) is uninduced formation rate or 7α OHT (observed in
in vitro experiment)
FORM7A = THETA(16)            ;Linear increase in 7α OHT producing enzyme over time

;;;;;;INDUCTION 16α-OHT, Combination of 2α OHT inhibition and 16β OHT induction
C2C16A = THETA(20)            ;amount of substrate that forms 16α OHT compared to 2A OHT
C2B16A =THETA(33)             ;amount of substrate that forms 16α OHT compared to 16B OHT
A_0(8) =C2C16A*RIN2A/K2A      ;Assumes 0 activity of 16β OHT producing enzyme at time 0

KMIND = THETA(24)             ;Amount of PB causing 50% of maximal induction

FE1  = THETA(25)/(THETA(25)+1);Fraction of PB CL following time course of 2α OHT
FE2= 1/(THETA(25)+1)          ;Fraction of PB CL following time course of and. induction

;;;;;; DIFFERENTIAL EQ
$DES
E1 = FE1*A(4)/A04             ;A(4)/A04 = 2α OHT producing enzyme activity compared to
uninhibited state.
E2 = FE2*A(10)/A010           ;A(10)/A010 = Androstenedione producing enzyme activity
compared to uninduced state.

PBACT = E1+E2                ;PB CL changes with activity of 2α OHT and andr. producing
enzyme
CL      = TVCL*PBACT         ; PB Clearance
K       = CL/V

DADT(1) = -KA*A(1)                                          ;PB Dosing compartment
DADT(2) = -K*A(2)+KA*A(1)                                   ;PB Central compartment
DADT(3) = RINRES*(1+(INDRES*A(2))/(KMIND+A(2))) -KRES*A(3)  ;Resorufin act. compartment
DADT(4) = RIN2A -K2A*A(4)*(1+(IND2A*A(2))/(KMIND+A(2)))     ;2α-OHT act. compartment
DADT(5) = RIN2B*(1+(IND2B*A(2))/(KMIND+A(2))) -K2B*A(5)     ;2β-OHT act. compartment
DADT(6) = RIN6A*(1+(IND6A*A(2))/(KMIND+A(2))) -K6A*A(6)     ;6α-OHT act. compartment
DADT(7) = FORM7A                                            ;7α-OHT act. compartment
DADT(8) = C2C16A*RIN2A+C2B16A*RIN16B*(1+(IND16B*A(2))/(KMIND+A(2)))-
K2A*A(4)*(1+(IND2A*A(2))/(KMIND+A(2)))-K16B*A(9)            ;16α-OHT act. compartment
DADT(9) = RIN16B*(1+(IND16B*A(2))/(KMIND+A(2)))-K16B*A(9)   ;16β-OHT act. compartment
DADT(10) = RINAND*(1+(INDAND*A(2))/(KMIND+A(2))) -KAND*A(10) ;Androstenedione act. comp.
```

Appendix